SUPPORTING INFORMATION

Chiral recognition and efficient enantiopurification of L-lactic acid by diastereomeric crystallization

Yuanyuan Shen,[a] Ying Liu,*[a] Zexiang Ding,[a] Jiaqi Li,[a] Rundao Chen,[a] Feng Zhou,[b] Lihang Chen,[c] Qimei Sun,[b] Yuli Bai,[b] Zhiguo Zhang,[ac] Qiwei Yang,[ac] Kai Qiao,[b] Qilong Ren,[ac] and Zongbi Bao*[ac]

[a] Key Laboratory of Biomass Chemical Engineering of Ministry of Education, College of Chemical and Biological Engineering, Zhejiang University, Hangzhou 310058, Zhejiang, P. R. China.

[b] SINOPEC Dalian Research Institute of Petroleum and Petrochemicals Co., Ltd., Dalian 116045, Liaoning, P. R. China.

[c] Institute of Zhejiang University-Quzhou, Quzhou 324000, Zhejiang, P. R. China.

Supplementary Text

S1 Phase Equilibrium Data Fitting

(1) Modified Apelblat Equation: Derived from the Clausius-Clapeyron equation, the modified Apelblat equation is a widely used semi-empirical model for correlating solubility with temperature in pure solvents[1,2]:

$$\ln x_1 = a + \frac{b}{T/\mathrm{K}} + c\ln\frac{T}{\mathrm{K}} \quad (1)$$

Where x_1 is the mole-fraction solubility of (R)-1-PA-D/L-LA crystal or (R)-1-PEA-D/L-LA crystal; T stands for the absolute temperature, and a, b, and c are fitting parameters.

(2) Buchowski-Ksiazaczak λh Equation: The λh equation, developed by Buchowski et al., describes solubility in hydrogen-bonded systems using two parameters (λ and h)[3,4]:

$$\ln\left(1+\frac{1-x_1}{x_1}\right) = \ln\left(\frac{1}{T}-\frac{1}{T_\mathrm{m}}\right) \quad (2)$$

Where T_m denotes the melting temperature.

To quantitatively describe the solubility behavior and evaluate the applicability of thermodynamic models, the experimental data were fitted using both the modified λh equation and the Apelblat model via nonlinear regression in MATLAB 2020a. Model accuracy was evaluated using the Average Relative Deviation (RAD) and Root Mean Square Deviation (RMSD):

$$\mathrm{RAD} = \frac{100}{N}\times\sum_{i=1}^{N}\left|\frac{x_i^{\mathrm{exp}} - x_i^{\mathrm{cal}}}{x_i^{\mathrm{exp}}}\right| \quad (3)$$

$$\mathrm{RMSD} = \left[\frac{1}{N}\times\sum_{i=1}^{N}\left(x_i^{\mathrm{exp}} - x_i^{\mathrm{cal}}\right)^2\right]^{1/2} \quad (4)$$

Where N is the number of experimental data points, x^{exp}_i and x^{cal}_i denote the experimentally measured and model-calculated solubility values, respectively. **Table S4** shows the solubility of four chiral salts in MeCN using λh and Apelblat model parameters.

The Apelblat model provided superior accuracy across all systems, particularly for (R)-1-PEA-L-LA (RAD = 2.13%, RMSD = 2.72%), indicating highly regular solubility behavior and strong thermodynamic consistency in MeCN. By contrast, the λh model exhibited notable deviation for (R)-1-PA-L-LA (λ = 0.69), suggesting pronounced non-ideal behavior, likely due to strong solute-solvent interactions or complex intermolecular forces in the crystalline lattice. These solubility trends and model evaluations provide a foundation for further thermodynamic analysis of the dissolution process.

(3) Thermodynamic properties of the dissolution process: The solute-specific thermodynamic parameters, ΔH_{sol}, ΔS_{sol} and ΔG_{sol} were determined from a van't Hoff analysis of the solubility data[5,6]:

$$\frac{\Delta H_{\mathrm{sol}}}{R} = -\frac{\partial \ln x}{\partial\left(\frac{1}{T}-\frac{1}{T_{\mathrm{hm}}}\right)} \tag{5}$$

$$\Delta G_{\mathrm{sol}} = -RT_{\mathrm{hm}} \times \text{intercept} \tag{6}$$

$$\Delta S_{\mathrm{sol}} = \frac{\Delta H_{\mathrm{sol}} - \Delta G_{\mathrm{sol}}}{T_{\mathrm{hm}}} \tag{7}$$

Where ln x represents the natural logarithm of the solute mole fraction, Thm represents thermodynamic equilibrium temperature of dissolution, and the intercept is obtained from the linear regression of ln x as a function of $\left(\frac{1}{T}-\frac{1}{T_{hm}}\right)$. The thermodynamic data for the dissolution process of the four crystalline salts in MeCN are summarized in **Table S5**. All ΔH_{sol} values are positive, indicating that the dissolution of all four crystalline salts in MeCN is endothermic, while all ΔG_{sol} values are positive, indicating that the dissolution process is non-spontaneous under standard conditions. The positive ΔG_{sol} is predominantly governed by the unfavorable enthalpy change ($\Delta H_{sol} > 0$), whereas the positive entropy change ($\Delta S_{sol} > 0$) contributes favorably but is insufficient to overcome the enthalpic barrier. Consequently, although the dissolution is thermodynamically endothermic and non-spontaneous, the enthalpic contribution dominates, resulting in positive free energy changes. At ambient temperature, the dissolution process of these four crystalline salts in MeCN is non-spontaneous; achieving spontaneous dissolution may require tuning the solvent, temperature, or other operational parameters to modify the thermodynamic characteristics and promote the process.

(4) Wilson Model: The Wilson activity coefficient model describes the non-ideal mixing behavior of liquids[7]. Neglecting pressure effects, the solubility in a solid-liquid equilibrium system can be expressed as:

$$\ln(\gamma_1 x_1) = -\frac{\Delta_{fus}H_m}{R}\left(\frac{1}{T}-\frac{1}{T_m}\right) \tag{8}$$

Where γ_1 is the activity coefficient of the solute, $\Delta_{fus}H_m$ is the molar melting enthalpy, and the T_m is the melting temperature. For a ternary system, the Wilson equation is written as:

$$\ln\gamma_i = 1 - \ln\left(\sum_{j=1}^{N} x_j \Lambda_{ij}\right) - \sum_{k=1}^{N}\left(\frac{x_k \Lambda_{ki}}{\sum_{j=1}^{N} x_j \Lambda_{ki}}\right) \tag{9}$$

$$\Lambda_{ij} = \frac{V_j}{V_i}\exp\left(-\frac{\lambda_{ij}-\lambda_{ii}}{RT}\right) = \frac{V_j}{V_i}\exp\left(-\frac{\Delta\lambda_{ij}}{RT}\right) \tag{10}$$

Where Λ_{ij} is the Wilson parameter related to the pure-component molar volumes V_i and V_j, thermodynamic temperature, and intermolecular interaction energies; and $\Delta\lambda_{ij}$ represents cross-interaction paramete between components i and j.

(5) NRTL Model: The Non-Random Two-Liquid (NRTL) model, proposed by Renon and Prausnitz in 1968, accounts

for non-random molecular distributions in liquid mixtures by modifying the local composition expression[8]:

$$\ln \gamma_i = \frac{\sum_{j=1}^{N} x_j \tau_{ji} G_{ji}}{\sum_{k=1}^{N} x_k G_k} + \sum_{j=1}^{N} \frac{x_j G_{ji}}{\sum_{k=1}^{N} x_k G_k} \left(\tau_{ji} - \frac{\sum_{k=1}^{N} x_k \tau_{kj} G_{kj}}{\sum_{k=1}^{N} x_k G_{kj}} \right) \quad (11)$$

$$G_{ji} = \exp(\alpha_{ij} \tau_{ij}) \quad (12)$$

$$\alpha_{ij} = \alpha_{ji} = \alpha \quad (13)$$

$$\tau_{ij} = \frac{g_{ij} - g_{jj}}{RT} = \frac{g_{ij}}{RT} \quad (14)$$

Where τ_{ij} is the NRTL interaction parameter related to temperature and intermolecular interactions, α is the non-randomness factor (typically 0.2-0.47)[9], and Δg_{ij} represents cross-interaction parameter between components *i* and *j*.

To accurately extend the binary system parameters to the ternary system, the Wilson and NRTL parameters are expressed as:

$$\Lambda_{ij} = \frac{V_j}{V_i} \exp\left[-\left(a_{ij} + \frac{b_{ij}}{T} \right) \right] \quad (15)$$

$$\tau_{ij} = a_{ij} + \frac{b_{ij}}{T} \quad (16)$$

Where a_{ij} and b_{ij} represent the interaction parameters optimized via nonlinear regression of solubility data, treated as constant independent of temperature and composition.

Nonlinear regression of the ternary phase equilibrium data was performed in Python using the Wilson and NRTL thermodynamic models. Optimized interaction parameters provided a robust framework for correlating and predicting solubility behavior. For the (R)-1-PA-D-LA/(R)-1-PA-L-LA/MeCN ternary system, solid-liquid equilibrium data were well described by both models, with maximum RAD and RMSD values of 8.80% and 0.69% for Wilson, and 14.09% and 0.61% for NRTL, respectively, demonstrating good agreement with experimental measurements (**Table S5**).

Correlation analyses between the experimental and predicted values indicate excellent agreement for both models (**Fig. S15**), with linear regression slopes close to unity and R^2 values approaching 1. For instance, in the Wilson model:

$w^{pre} = (0.9538 \pm 0.0215)\ w^{exp} + 0.00211$ R^2=0.9843 (R)-1-PA-D

$w^{pre} = (0.9815 \pm 0.0154)\ w^{exp} + 0.00211$ R^2=0.9925 (R)-1-PA-L

$w^{pre} = (0.9815 \pm 0.0132)\ w^{exp} + 0.00211$ R^2=0.9944 MeCN

Similarly, for the NRTL model:

$w^{pre} = (0.9002 \pm 0.0302)\ w^{exp} + 0.00211$ R^2=0.9663 (R)-1-PA-D

$w^{pre} = (0.9906 \pm 0.0131)\ w^{exp} + 0.00211$ R^2=0.9946 (R)-1-PA-L

$w^{pre} = (0.9585 \pm 0.0131)\ w^{exp} + 0.00211$ R^2=0.9943 MeCN

Here, wpre and wexp represent the calculated and experimental values, respectively. The close-to-unity slopes and high R^2 values confirm excellent agreement between experimental and calculated data, demonstrating that the Wilson and NRTL models, along with their optimized parameters, can reliably predict solubility behavior in ternary systems.

S2 Hirshfeld Surface Analysis and 2D Fingerprint Plots of Chiral Salts

Hirshfeld surface analysis provides a quantitative and intuitive means to investigate the nature and spatial distribution of weak intermolecular interactions within crystals. The electron density mapped on the Hirshfeld surface reflects the relative strength of these interactions: regions colored red indicate high electron density, corresponding to stronger intermolecular interactions; white regions correspond to intermediate electron density, predominantly representing weaker intermolecular interactions, including C-H···O and C-H···N hydrogen bonds, as well as dispersive forces and π-π stacking between molecules; blue regions denote near-zero electron density, indicating weak or negligible intermolecular contacts. This color-coded representation offers a clear framework for identifying the dominant types of intermolecular interactions and for elucidating the microscopic interactions governing the overall crystal packing.

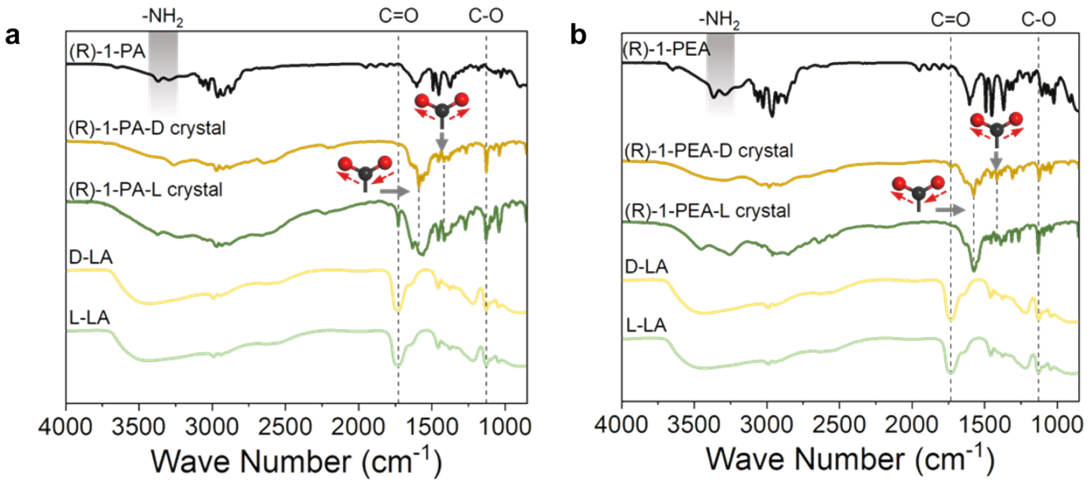

Fig. S1 FTIR spectra of the four crystalline salts: (a) (R)-1-PA-D/L crystal formed by (R)-1-PA and D/L-LA, (b) (R)-1-PEA-D/L crystal formed by (R)-1-PEA and D/L-LA.

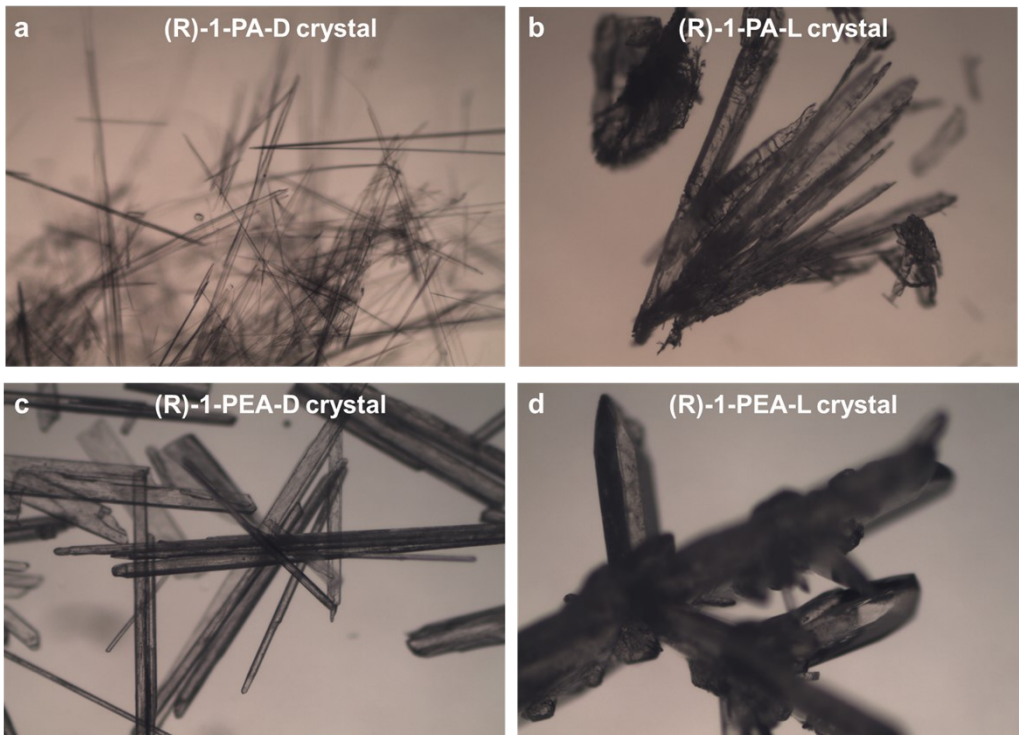

Fig. S2 Optical micrographs of the four crystalline salts. (a) (R)-1-PA-D crystal; (b) (R)-1-PA-L crystal; (c) (R)-1-PEA-D crystal; (d) (R)-1-PEA-L crystal.

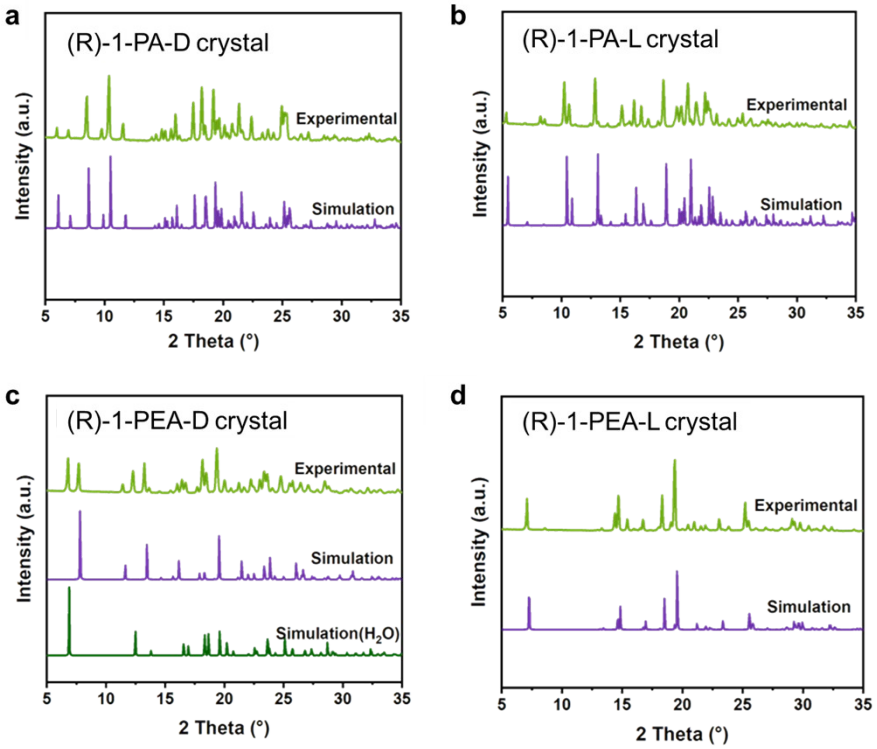

Fig. S3 Comparison of simulated PXRD patterns derived from single-crystal structures with experimental PXRD patterns of samples. (a) (R)-1-PA-D crystal; (b) (R)-1-PA-L crystal; (c) (R)-1-PEA-D crystal; (d) (R)-1-PEA-L crystal.

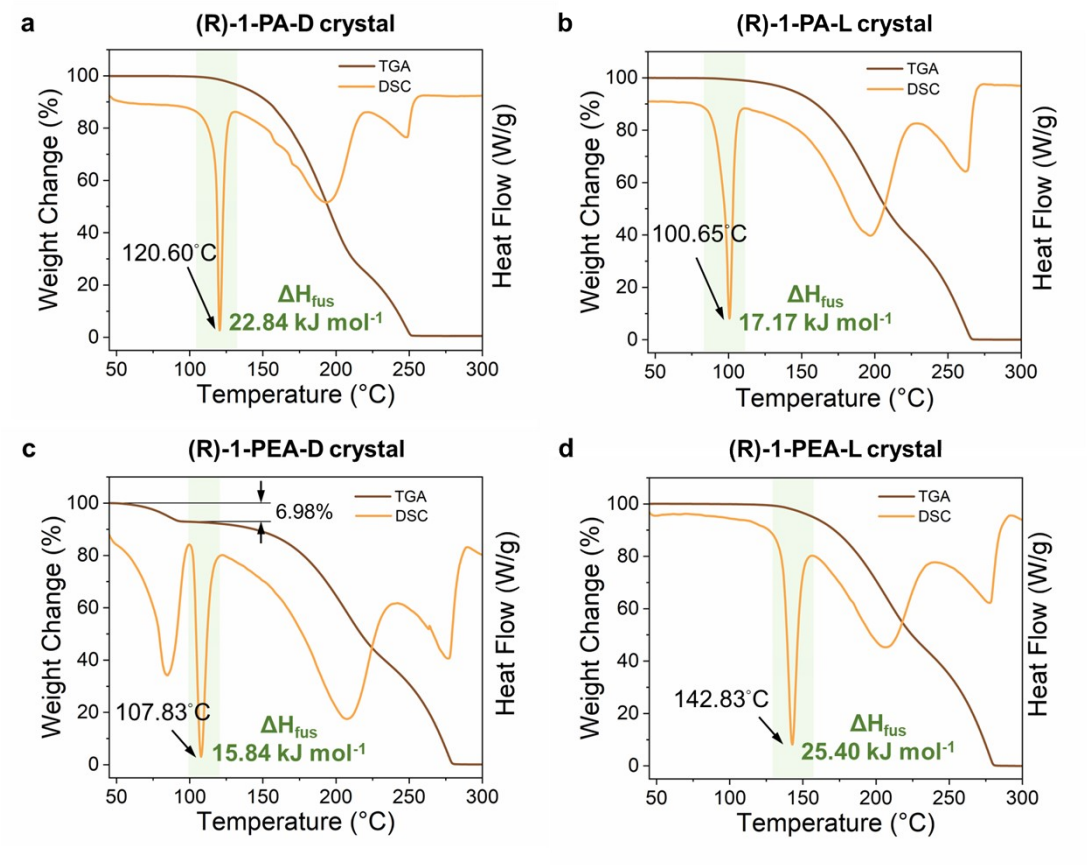

Fig. S4 TGA-DSC profiles of the four crystalline salts: (a) (R)-1-PA-D crystal, (b) (R)-1-PA-L crystal, (c) (R)-1-PEA-D crystal, and (d) (R)-1-PEA-L crystal.

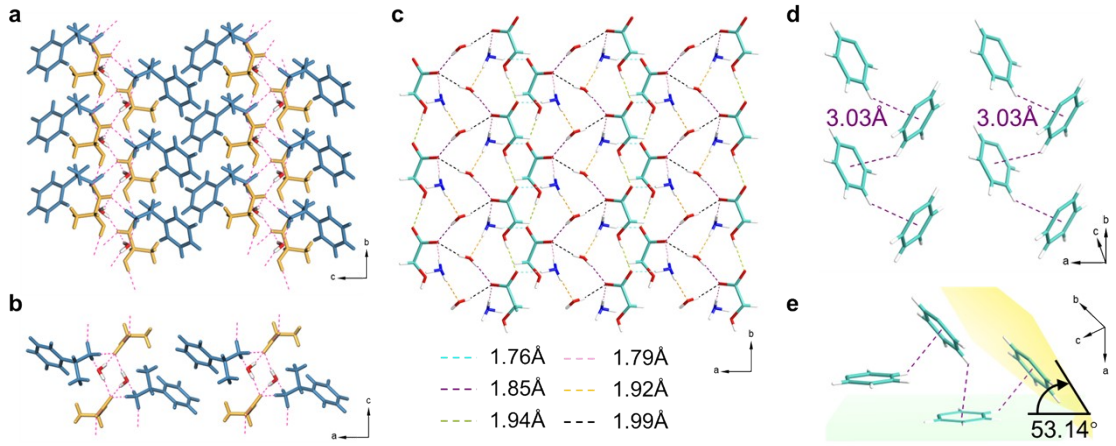

Fig. S5 Schematic representation of the structural characterization of the (R)-1-PEA-D·H_2O crystal.

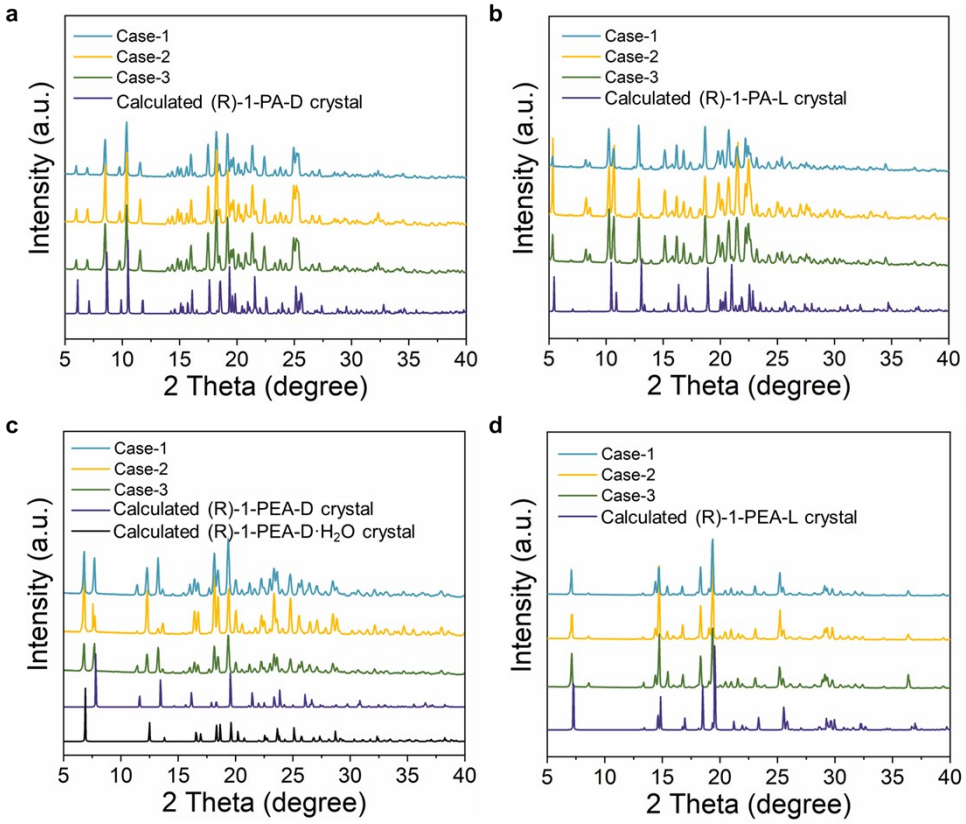

Fig. S6 Comparison of PXRD patterns of diastereomeric salts under different crystallization conditions. (a) (R)-1-PA-D crystal; (b) (R)-1-PA-L crystal; (c) (R)-1-PEA-D crystal; (d) (R)-1-PEA-L crystal.

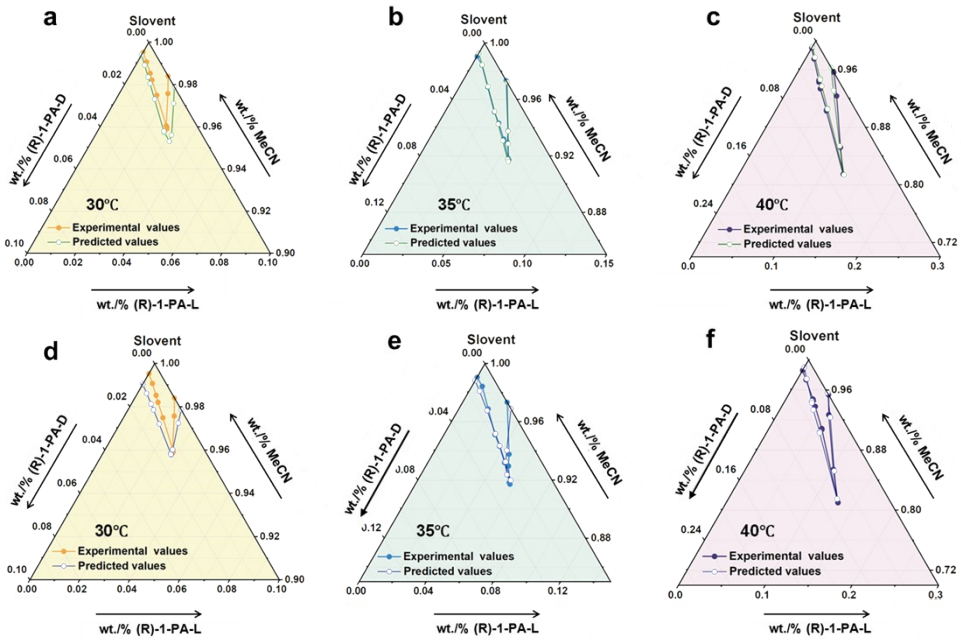

Fig. S7 Experimental versus model-predicted ternary phase behavior of the (R)-1-PA-D (1) / (R)-1-PA-L (2) / MeCN (3) system. (a-c) Wilson model, (d-f) NRTL model.

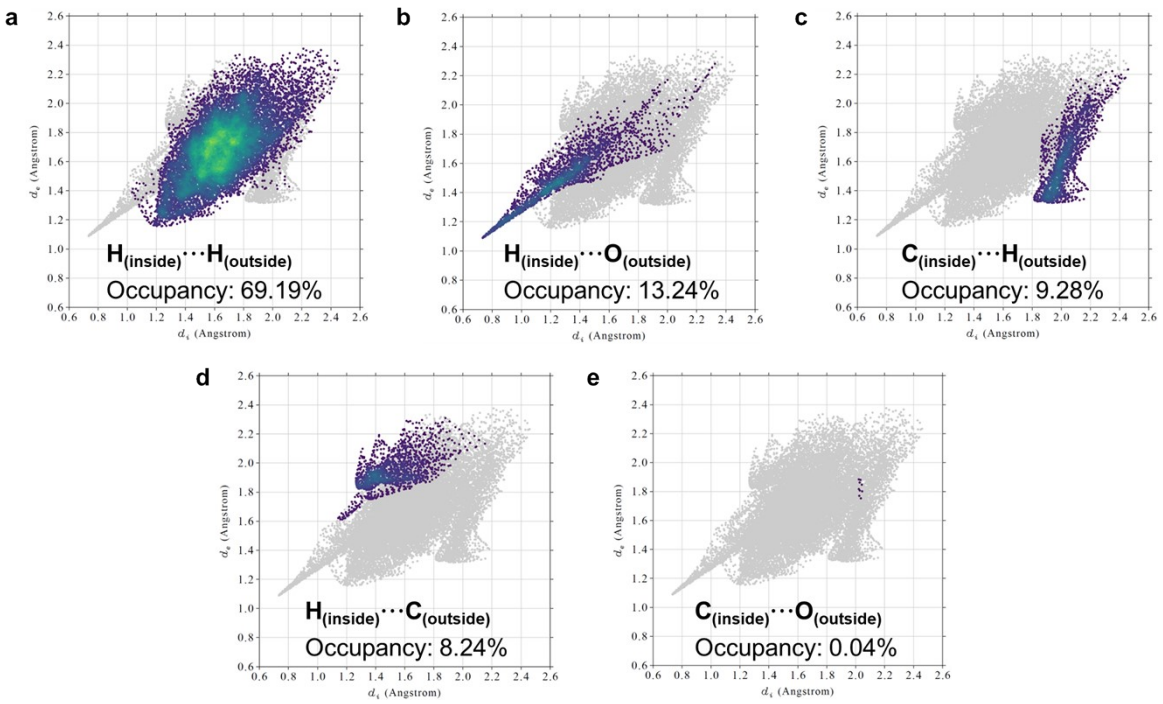

Fig. S8 Localized (magnified) region of the 2D fingerprint plot for (R)-1-PA-D crystal.

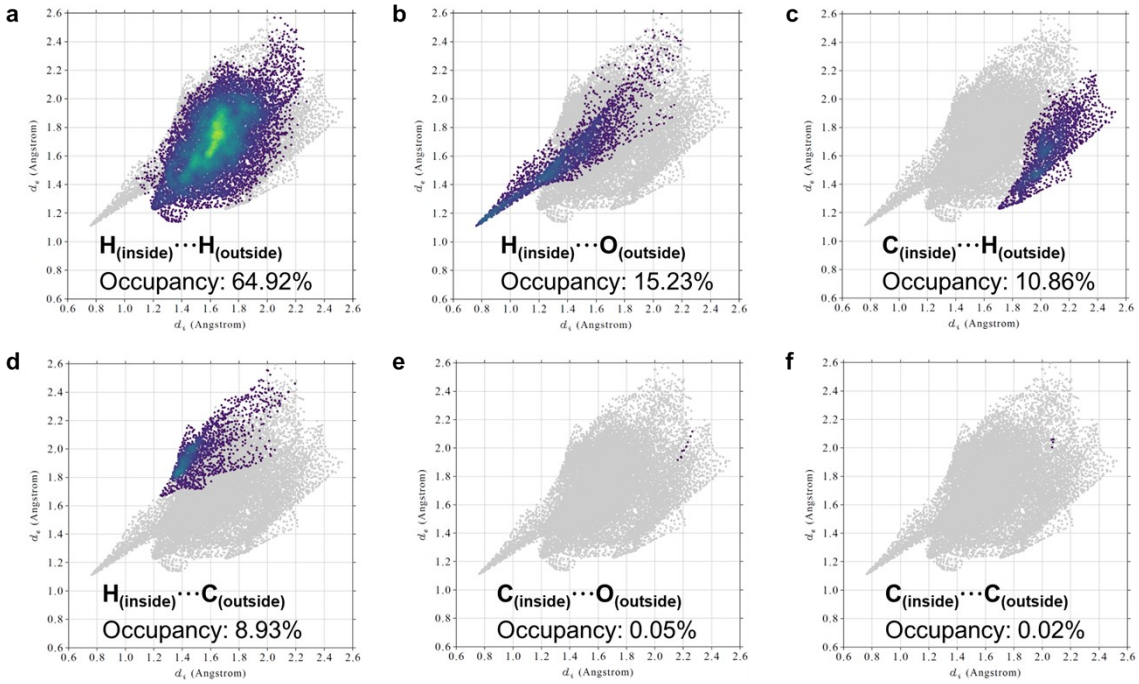

Fig. S9 Localized (magnified) region of the 2D fingerprint plot for (R)-1-PA-L crystal.

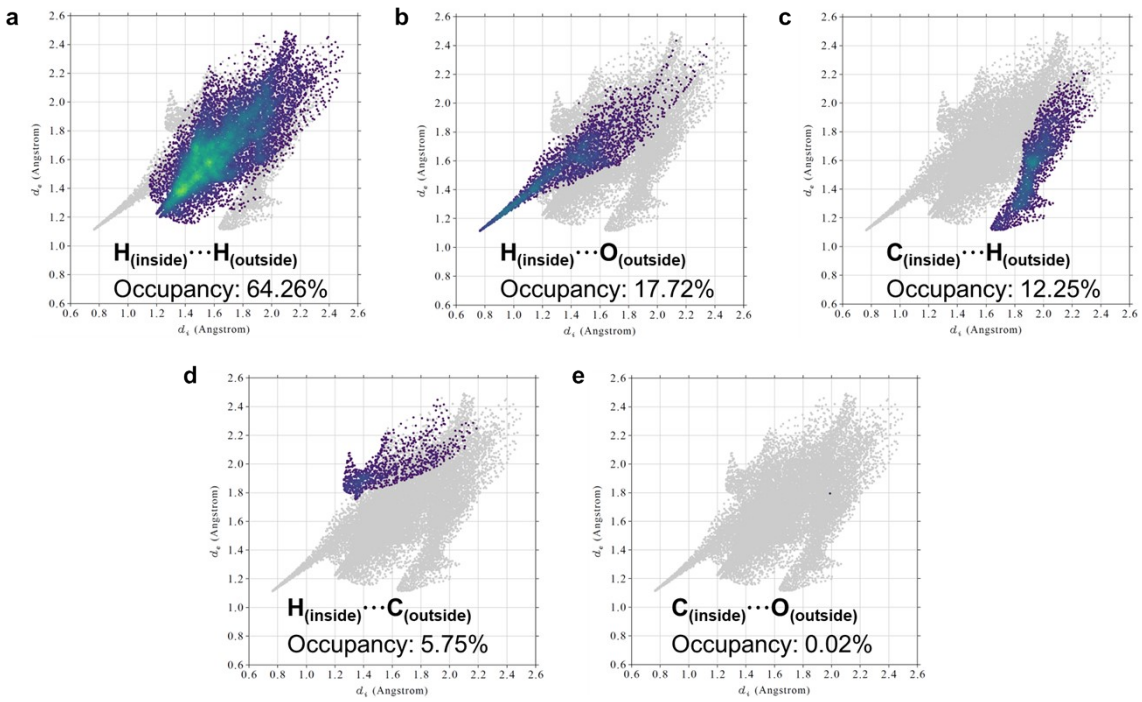

Fig. S10 Localized (magnified) region of the 2D fingerprint plot for (R)-1-PEA-D crystal.

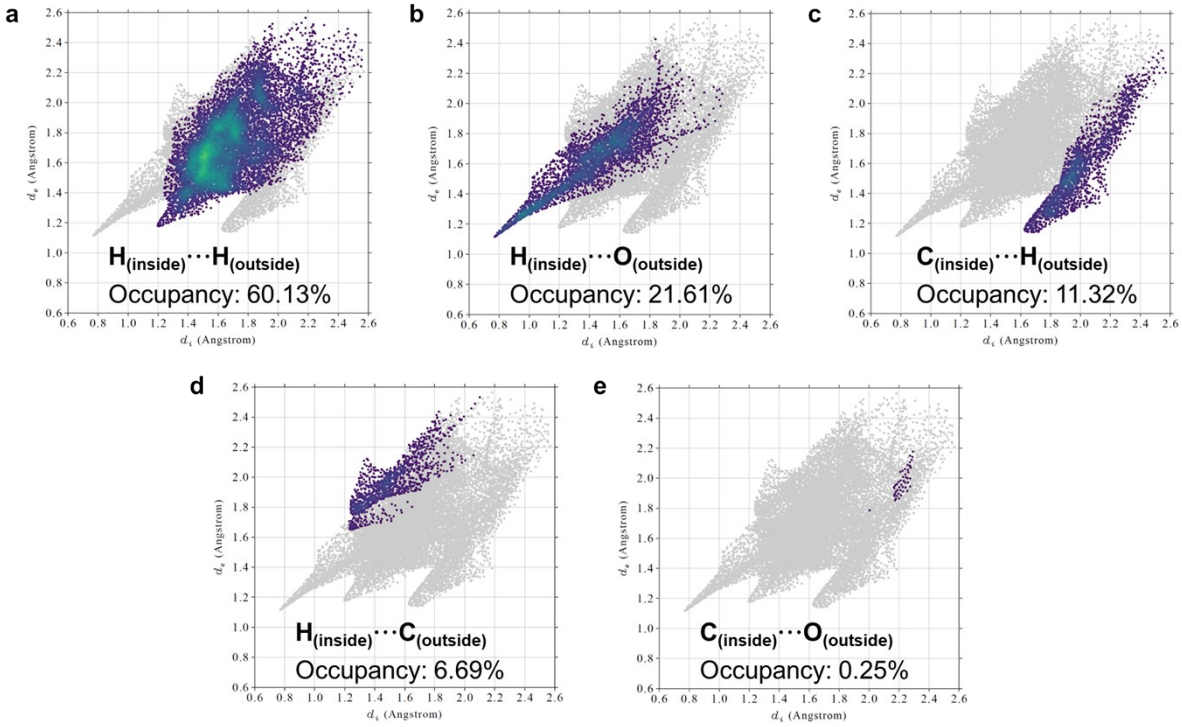

Fig. S11 Localized (magnified) region of the 2D fingerprint plot for (R)-1-PEA-L crystal.

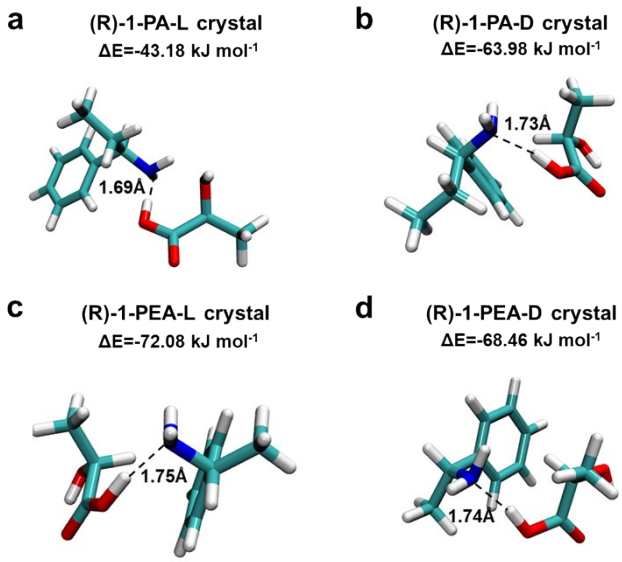

Fig. S12 Relative conformations and corresponding binding energies of chiral resolving agents complexed with D/L-LA under solvent-free conditions.

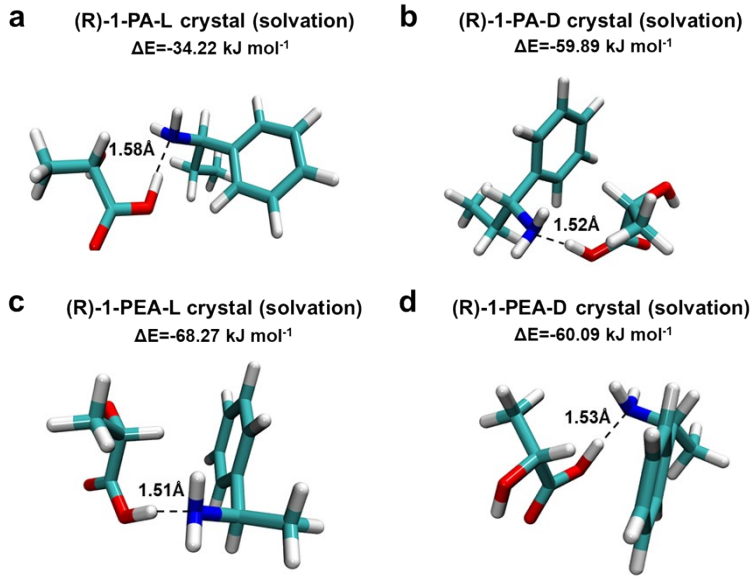

Fig. S13 Relative conformations and corresponding binding energies of chiral resolving agents complexed with D/L-LA under solvated conditions.

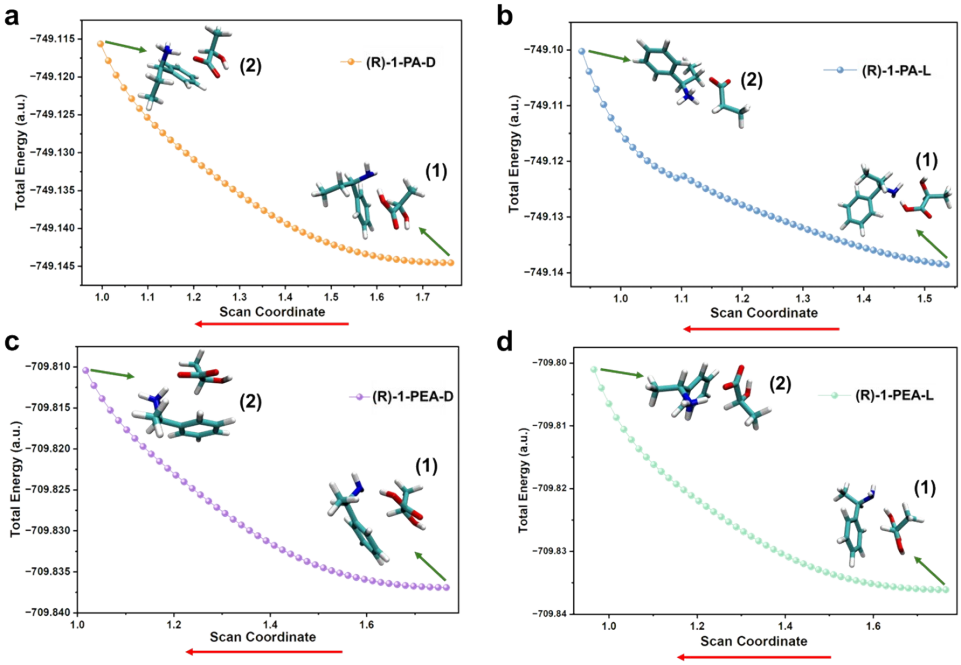

Fig. S14 Proton transfer from lactic acid to a chiral resolving agent under solvent-free conditions: flexible scan energy profile.

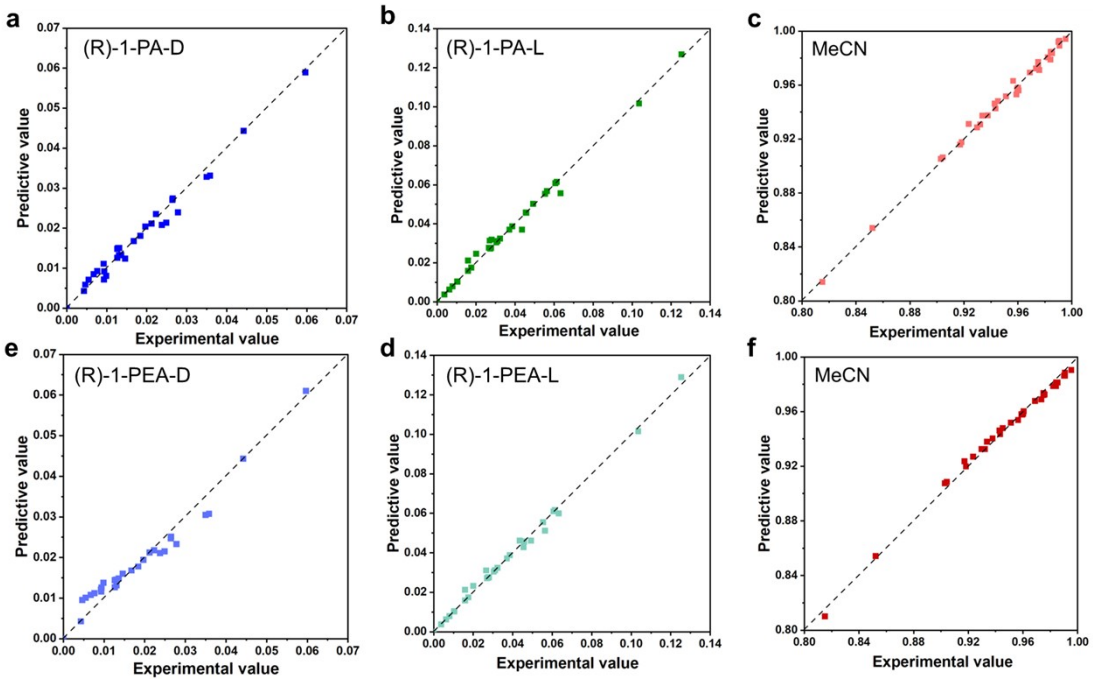

Fig. S15 Statistical correlation analysis between predicted and experimental values using the Wilson and NRTL models. (a-c) Wilson model, (d-f) NRTL model.

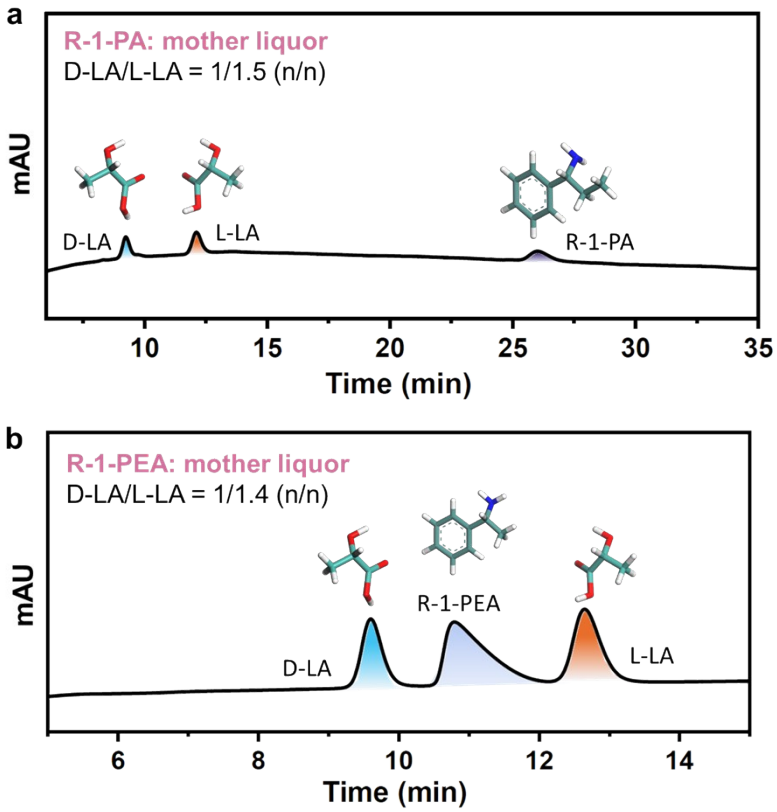

Fig. S16 Enantiomeric excess of lactic acid in the mother liquor during diastereomeric crystallization with different resolving agents. (a) (R)-1-PA system, (b) (R)-1-PEA system.

Table S1. Detailed characterization of chemicals utilized in this study.

Chemical	CAS No.	Purity a	Suppliers b	pKa	Molecular structure
D-LA	10326-41-7	≥90.0 wt.%	Aladdin	/	
L-LA	79-33-4	≥90.0 wt.%	Aladdin	/	
DL-LA	598-82-3	≥90.0 wt.%	Aladdin	/	
MeCN	75-05-8	≥99.0 wt.%	China National Pharmaceutical Group Chemical Reagents	/	
(R)-1-PA	3082-64-2	≥99.0 wt.%	Aladdin	9.34	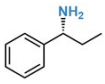
(R)-1-PEA	3886-69-9	≥98.0 wt.%	TCI	9.80	
(S)-1-PA	3789-59-1	≥99.0 wt.%	Aladdin	9.34	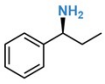
(S)-1-PEA	2627-86-3	≥99.0 wt.%	Sigma-Aldrich	9.80	
(S)-1-CPEA	195604-39-8	≥95.0 wt.%	Aladdin	10.10	
(R)-1-CPEA	6240-96-6	≥96.0 wt.%	Macklin	10.87	
(D)-Prol	68832-13-3	≥98.0 wt.%	Aladdin	14.77	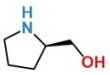
(L)-Prol	23356-96-9	≥97.0 wt.%	Sigma-Aldrich	14.77	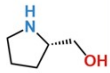
(D)-PPA	5267-64-1	≥98.0 wt.%	Aladdin	12.85	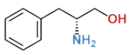
(L)- PPA	3182-95-4	≥98.0 wt.%	TCI	12.85	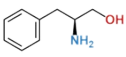

Note: D-lactic acid (D-LA); L-lactic acid (L-LA); DL-lactic acid (DL-LA); Acetonitrile (MeCN); (R)-1-phenylpropy lamine ((R)-1-PA); (R)-1-phenylethylamine ((R)-1-PEA); (S)-1-phenylpropylamine ((S)-1-PA); (S)-1-phenylethylamine ((S)-1-PEA); (S)-1-Cyclopropylethylamine ((S)-CPEA), (R)-1-Cyclopropylethylamine ((R)-1-CPEA); (D)-Prolinol ((D)-Prol), (L)-Prolinol ((L)-Prol), (D)-Phenylalaninol ((D)-PPA), (L)-Phenylalaninol ((L)-PPA).

Table S2. Single-crystal structure data of the crystalline salts.

Name	(R)-1-PA-D	(R)-1-PA-L	(R)-1-PEA-D	(R)-1-PEA-D·H_2O	(R)-1-PEA-L
formula	$C_{12}H_{19}NO_3$	$C_{12}H_{19}NO_3$	$C_{11}H_{17}NO_3$	$C_{11}H_{19}NO_4$	$C_{11}H_{17}NO_3$
MW(g/mol)	225.28	225.28	211.26	229.27	211.26
T/K	150 K	150 K	150 K	150 K	150 K
Crystal system	orthorhombic	orthorhombic	orthorhombic	Monoclinic	orthorhombic
Space group	$P2_12_12_1$	$P2_12_12_1$	$P2_12_12_1$	$P2_1$	$P2_12_12_1$
a(Å)	5.7873(3)	5.7543(1)	6.2722(5)	8.0904(3)	6.8466(7)
b(Å)	17.8836(6)	13.5274(2)	8.0783(6)	5.8849(3)	6.98240(8)
c(Å)	24.8439(14)	32.4808(5)	22.6180(2)	12.8722(5)	24.3030(2)
α(deg)	90	90	90	90	90
β(deg)	90	90	90	94.576(4)	90
γ(deg)	90	90	90	90	90
V($Å^3$)	2571.3(2)	2528.33(7)	1146.03(16)	610.91(5)	1161.83(2)
Z	8	8	4	2	4
ρ_{calc}(g/cm^3)	1.164	1.184	1.224	1.246	1.208
μ(mm^{-1})	0.677	0.689	0.728	0.783	0.718
Rc	0.0496	0.0554	0.0260	0.0494	0.0279
CCDC	2491484	2491485	2491489	2491491	2491490

Table S3. Lattice energies of the diastereomeric salts.

Name	Lattice energies
(R)-1-PA-D	332.92 kcal mol^{-1}
(R)-1-PA-L	286.60 kcal mol^{-1}
(R)-1-PEA-D	221.79 kcal mol^{-1}
(R)-1-PEA-L	229.04 kcal mol^{-1}

Table S4. Apelblat model parameters and λh coefficients describing the solubility of diastereomeric salts in MeCN.

	(R)-1-PA-D	(R)-1-PA-L	(R)-1-PEA-D	(R)-1-PEA-L
λ	0.0929	0.6948	0.3418	0.1345
h	64802.8076	11963.6551	20402.7352	44726.7081
10^2RAD	7.0328	19.9103	18.1141	3.1237
10^4RMSD	2.0224	43.1647	28.8173	0.6703
A	-272.9856	-1198.6424	-1082.1359	136.4494
B	6601.3488	45745.9434	41672.4115	-11521.9152
C	42.7405	182.3493	164.3552	-18.4551
10^2RAD	6.2585	6.6019	5.7217	2.1318
10^4RMSD	1.1639	10.7873	8.4850	0.2715

Table S5. Thermodynamic model parameters (NRTL and Wilson) for the ternary system comprising (R)-1-PA-D (1), (R)-1-PA-L (2), and MeCN (3).

Model parameters				RMSD%	R^2	α
			NRTL			
a_{12}	-0.142690	b_{12}	-770.878104	0.3847	0.9946	0.4
a_{21}	4.657114	b_{21}	442.262431			
a_{13}	7.222929	b_{13}	1948.442304	0.5448	0.9999	0.2
a_{31}	-0.738309	b_{31}	1479.913205			
a_{23}	-5.281135	b_{23}	1351.219489	0.6139	0.9999	0.3
a_{32}	0.784104	b_{32}	1156.569817			
30℃	RAD%			14.0860		
35℃	RAD%			4.2780		
40℃	RAD%			4.7532		
			Wilson			
a_{12}	-0.122493	b_{12}	-4.319370	0.2788	0.9972	
a_{21}	-5.399511	b_{21}	966.928482			
a_{13}	2.904757	b_{13}	116.560489	0.2523	0.9999	
a_{31}	-0.014744	b_{31}	528.513854			
a_{23}	3.101540	b_{23}	-445.745719	0.6942	0.9999	
a_{32}	4.897008	b_{32}	500.723683			
30℃		RAD%			8.7974	
35℃		RAD%			1.8045	
40℃		RAD%			4.2044	

Table S6. Number of molecules in MD simulations at varying composition ratios.

Name	[(R)-1-RA]	[(R)-1-REA]	[D-LA]	[L-LA]	MeCN
(R)-1-PA-D	61	-	61	-	24000
(R)-1-PA-L	428	-	-	428	24000
(R)-1-PEA-D	-	484	484	-	24000
(R)-1-PEA-L	-	53	-	53	24000

Table S7. Representative experimental material balance for the integrated reaction-crystallization-distillation process used for the upgrading of low-grade L-LA.

	Value
Reaction and crystallization section	
Total lactic acid feed	4.00 g
L-LA	3.60 g
D-LA	0.40 g
(R)-1-PA	6.00 g
MeCN	50 mL
Reaction temperature	60 ℃
Reaction time	2 h
Crystallization temperature	60 → 10-20 ℃
Crystallization yield	70%
ee of L-LA in isolated crystalline salt	>99%
Vacuum distillation section	
Dry crystalline salt	7.00 g
Theoretical lactic acid content in the salt	2.80g
Theoretical (R)-1-PA content in the salt	4.20g
Distillation temperature	200 ℃
System pressure	2 kPa
Bottom product (L-LA+(R)-1-PA)	2.77 g
Calculated (R)-1-PA content in the bottom product	0.34 g
ee of L-LA in bottom product	≥ 99%
Recovered (R)-1-PA (distillate/head fraction)	2.73 g
Recovery of (R)-1-PA	65%
Residual (R)-1-PA concentration in SP-3 sample	1.217 mg mL^{-1}

Note: The reported "≥ 99%" value for the bottom product refers to the *ee* of L-LA, rather than the overall chemical purity of the sample.

References

1. A. Apelblat and E. Manzurola, Solubilities of L-aspartic, DL-aspartic, DL-glutamic, p-hydroxybenzoic, o-anisic, p-anisic, and itaconic acids in water from T= 278 K toT= 345 K, *J. Chem. Thermodyn.*, 1997, **29**, 1527-1533.
2. C. Du, Y. Luo, C. Huang and R. Li, Solubility measurement and thermodynamic model correlation of baclofen in 12 pure organic solvents, *J. Chem. Eng. Data*, 2022, **67**, 2655-2661.
3. X. Li, C. Du, Y. Cong, J. Wang and H. Zhao, Solubility determination and thermodynamic modeling of paclobutrazol in nine organic solvents from T= (278.15 to 318.15) K and mixing properties of solutions, *J. Chem. Thermodyn.*, 2017, **104**, 261-273.
4. A. Noubigh, A. Aydi, A. Mgaidi and M. Abderrabba, Measurement and correlation of the solubility of gallic acid in methanol plus water systems from (293.15 to 318.15) K, *J. Mol. Liq.*, 2013, **187**, 226-229.
5. M. J. Jozwiakowski, N. A. T. Nguyen, J. M. Sisco and C. W. Spancake, Solubility behavior of lamivudine crystal forms in recrystallization solvents, *J. Pharm. Sci-Us.*, 1996, **85**, 193-199.
6. M. J. Abualreish and A. Noubigh, Experimental study and correlation of the solid-liquid equilibrium of some amino acids in binary organic solvents, *Korean Chem. Eng. Res.*, 2024, **62**, 173-180.
7. A. Jouyban-Gharamaleki, The modified Wilson model and predicting drug solubility in water-cosolvent mixtures, *Chem. Pharm. Bull.*, 1998, **46**, 1058-1061.
8. H. Renon and J. M. Prausnitz, Local compositions in thermodynamic excess functions for liquid mixtures, *AIChE J.*, 1968, **14**, 135-144.
9. H. Renon and J. M. Prausnitz, Estimation of parameters for the NRTL equation for excess Gibbs energies of strongly nonideal liquid mixtures, *J. Ind. Eng. Chem.*, 1969, **8**, 413-419.